Journal of Technology and Innovative Knowledge

Journal Home Page: www.jotik.astu.edu.et

Research Article

Poly (vinyl alcohol)-Based Phase Inversion Membranes for Sodium-Ion Conducting Solid Polymer Electrolytes

Lemi Mikael [1], Lemessa Shibiru [1], Lalisa Dejene [1], Mekdes Mitiku [1] and Jung Yong Kim [1,2,*]

[1]Department of Materials Science and Engineering, Adama Science and Technology University, Adama P.O. Box 1888, Ethiopia
[2]Center of Advanced Materials Science and Engineering, Adama Science and Technology University, Adama P.O. Box 1888, Ethiopia
*Correspondence: jungyong.kim@astu.edu.et

Abstract: Poly (vinyl alcohol) (PVA)-based thin films can be utilized as an ion-conducting polymer electrolyte membrane for battery and supercapacitor when it incorporates a sodium salt such as Na_2SO_4. Hence, we fabricated the PVA/Na_2SO_4 membrane using the phase inversion method, for which ethanol was employed as a nonsolvent. Then we studied the structural, thermal, morphological and electrical properties of the PVA-based membranes using x-ray diffraction (XRD), thermogravimetric analysis (TGA) coupled with differential thermal analysis (DTA), optical microscopy (OM) and electrochemical impedance spectroscopy (EIS). Resultantly, the PVA/Na_2SO_4–based solid polymer electrolyte exhibited the ionic conductivity of ~2.0×10^{-7} S/cm. Furthermore, the electrochemical devices with the ITO/PVA(Na_2SO_4)/ITO configuration exhibited the electric double layer capacitance (EDLC) behavior with the energy storage of 9.2 μF/cm² (Na_2SO_4 0.5M) and 8.1 μF/cm² (Na_2SO_4 1.0 M) in the potential range of 0.0V to 1.2 V.

Keywords: solid polymer electrolyte; phase inversion membrane; poly (vinyl alcohol)

Citation: Mikael *et al.*, : Poly(vinyl alcohol)-Based Phase Inversion Membranes for Sodium-Ion Conducting Solid Polymer Electrolytes. *Journal of Technology and Innovative Knowledge*, 2024 (**1**):1

Academic Editor: Dr Ketema Tafess Tulu

Received: 16 February 2024
Revised: 19 April 2024
Accepted: 18 July 2024
Published: 19 August 2024

1. Introduction

Plastic membranes can serve as an ion-conducting polymer electrolyte for the energy storage and conversion devices such as batteries, supercapacitors, fuel cells, and photovoltaic devices (Kim & Chung, 2002; Kim et al., 2006). Polymer electrolytes have a number of benefits over conventional liquid electrolytes, which may include the enhanced safety, improved stability, and design flexibility (e.g., roll-to-roll processibility) with low cost (Drioli & Fontananova, 2012). However, finding a balance between the high ionic conductivity and the mechanical resilience with desirable interfacial properties is the major challenge in the development of polymer electrolytes (Wang et al., 2011). For example, polymer membranes can be modified to improve their ionic transport properties if appropriate plasticizers were employed into the system with a partial expense of their mechanical properties. Here, the properties of the polymer electrolytes depend on several factors such as molecular structure, polymer-salt complex morphology, segmental movement, salt lattice energy, and additive species such as plasticizers and fillers (Long et al., 2016). Recently, the high demand for efficient and sustainable electrochemical devices such as batteries and supercapacitors for electric vehicles has pushed researchers to further advance the polymer electrolyte technologies (Bae & Kim, 2021).

The phase inversion process is to transform a polymer membrane from a liquid state to a solid state in a controlled way. The solidification process is initiated through the liquid-liquid (L-L) demixing. In this demixing process, one of the liquid phases will solidify to

produce the solid matrix (Tavajohi & Khayet, 2024). The membrane morphology including vertically asymmetric microporous structures can be tailored by controlling the initial stage of L-L phase separation. In such a process, a polymer solution cast on an appropriate support is then subsequently immersed in a coagulation bath containing non-solvent (also called anti-solvent). The principle of phase separation is to exchange the solvent with a non-solvent via coagulation bath. However, both small molecular solvent and non-solvent are miscible together because of entropic gain, indicating the non-solvent can suck out the solvent molecules from the polymer membrane, i.e., solidification (Kahrs & Schwellenbach, 2020). Here, the structure of polymer membrane can be adjusted to have the oriented sponge or finger configurations by controlling the kinetics and thermodynamics parameters.

In this study, the porous poly (vinyl alcohol) (PVA) membrane was prepared by phase inversion method (Eljaddi et al., 2021). PVA is one of a few water-soluble polymers, affording an environmentally-friendly green process without using any toxic solvent. The polymer has excellent film-forming properties, i.e., tunability for versatile design applications. Hence, to date, many research groups have investigated the PVA membranes for the purpose of polymer electrolyte in a gel state (Gu & Wei, 2016; Wang et al., 2024; Sánchez-Valdez et al., 2023; Xiao et al., 2021; Taktar et al, 2020; Xie et al., 2020; Cheng et al., 2019; Li et al., 2018; Pendashteh et al., 2017; Batisse & Raymundo-Piñero, 2017) instead of a solid state, which is a different trend compared to the typical poly(ethylene oxide) (PEO)-based membranes (Kim & Bae, 1999a; Kim & Bae, 1999b; Hong et al., 2001). Hence, in this study, we focus on the solid polymer electrolyte (SPE) composed of PVA and Na_2SO_4 for the battery and supercapacitor applications (Kamcev & Freeman, 2016). Then, we investigate the structural, thermal, morphological and electrochemical properties of these PVA-based SPEs, for which we employ the instruments such as x-ray diffraction (XRD), thermogravimetric analysis coupled with differential thermal analysis (TGA/DTA), optical microscopy (OM), and potentiostat/galvanostat with the impedance analyzer for the electrochemical impedance spectroscopy (EIS) analysis.

2. Materials and Methods

2.1. Materials

PVA has the average number molecular weight (M_n) of 1,500 g/mol from Junsei Chemical Co., Japan, whereas sodium sulphate (Na_2SO_4) has molecular weight of 142.04 g/mol from Norbright industry Co., China. Deionized (DI) water was collected from the Materials Science and Engineering Lab at ASTU.

2.2. Preparation of Phase Inversion Membrane

The membrane formation process through the phase inversion method is shown in Figure 1. PVA asymmetric membranes were made by dissolving polymer (2g) into 20 mL deionized water. Then, for 24 hours, the solutions were constantly stirred at 550 rpm at 80 °C. After that, it was degassed for 5 hours at room temperature to remove any gas bubble. Finally, these solutions were cast onto glass plate with a film thickness of (~125 μm) and submerged in an ethanol coagulation bath. A thin layer of PVA asymmetric membrane is fabricated after 3 hours of precipitation. The asymmetric membrane was ultimately dried under ambient condition for 12 hours (Guillen et al., 2011; Wang & Lai, 2013; Sapalidis, 2020; Ahmad et al., 2012). Furthermore, to accommodate Na_2SO_4 salt in the aforementioned PVA membrane, the dried phase-inversion membrane was dipped into the 0.5 M or 1.0 M Na_2SO_4 bath and then after drying it under ambient condition, the membrane was sandwiched between two ITO glasses to make an electrochemical device with ITO/PVA(Na_2SO_4)/ITO configuration.

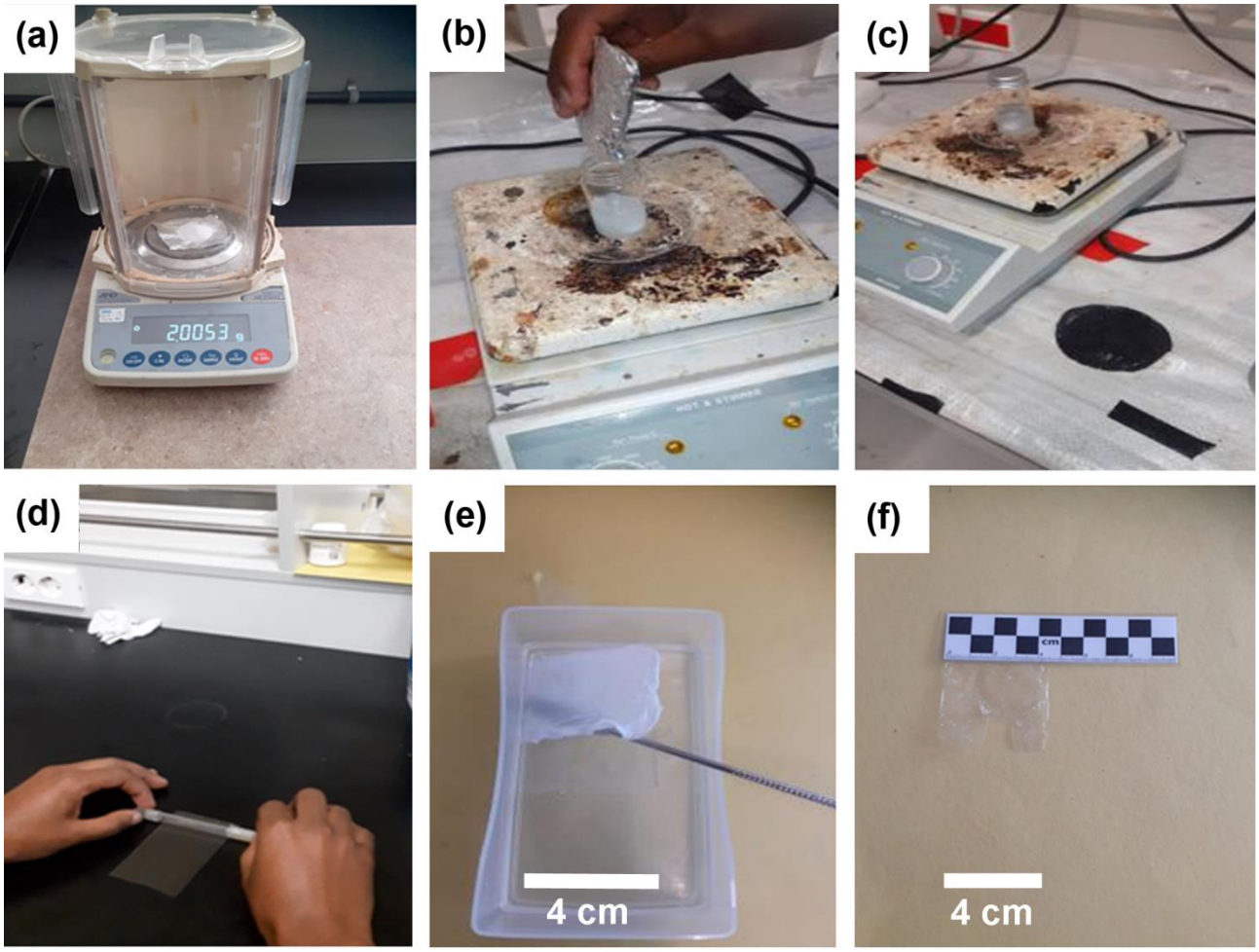

Figure 1. Membrane formation through phase-inversion process: (a) Measurement of 2g PVA, (b) Addition of PVA into 20 mL deionized water, (c) Stirring for 24 hours at 80 °C, (d) Membrane casting, (e) Dipping into the nonsolvent Ethanol bath, and (f) Phase-inversion membrane.

2.3. Characterization

The XRD data were obtained using the XRD-7000 x-ray diffractometer (SHIMADZU Corporation (Japan), with Cu-Kα radiation = 0.15418 nm, voltage = 40.0 (kV), current = 30.0 (mA), in the 2θ range between 5 ° and 45°, whereas the TGA/DTA data were captured using a differential thermal calorimetery (DTG-60H, Shimadzu, Japan) at a scan rate of 10 °C/min under N_2. Optical microscopy image was obtained using the Model: HR3-RF; HUVITZ Co., South Korea. The electrochemical impedance spectroscopy (EIS) analysis was carried out using the SP-300 potentiostat/galvanostat with an impedance analyzer (Bio-Logic, SAS, France) in the frequency range of 10 mHz to 100 KHz, whereas the charge density vs. voltage and the areal capacitance vs. voltage characteristics were obtained by using the SP-300 potentiostat/galvanostat at the voltage scan rate of 50 mV/sec.

3. Results and Discussion

The schematic ternary phase diagrams for 'solvent/nonsolvent/polymer' system composed of water, ethanol, and PVA is shown in Figure 2, explaining the phase inversion process of PVA membranes (Loeb & Sourirajan, 1963; Wienk et al., 1996). In this diagram, the binodal curve indicates the boundary between the one-phase and the two-phase (the unstable and metastable combined region) whereas the spinodal curve denotes the boundary between the meta-stable and unstable regions. Importantly, the blue line describes the overall membrane-formation pathway from the initial PVA solution (the point **A**) to the final membrane (the point **D**) via the phase-inversion (the point **B**) and solidification (the point **C**) processes. Specifically, the point **B** is the key step, in which the asymmetric membrane is formed with a porous structure because from the surface of the membrane, the water molecules can be effectively removed through the C_2H_5OH-H_2O mixing. Here, it is noteworthy that C_2H_5OH acts as a nonsolvent for PVA but a solvent for H_2O. Hence, through the mixing between C_2H_5OH and H_2O, the H_2O molecules could be removed from the PVA membrane. Note that Figure 2 is a general scheme applicable to any 'solvent/nonsolvent/polymer' system for phase-inversion membrane applications. The starting location (**A**) simply depends on the concentration of polymer, e.g., ~9 wt.% PVA in water in this study.

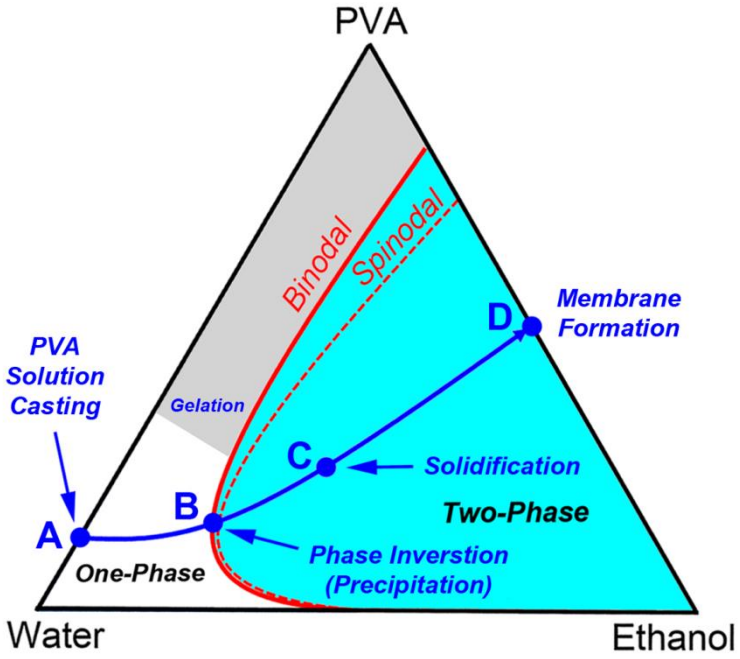

Figure 2. Schematic ternary phase diagram explaining the phase-inversion process during membrane formation.

Figure 3 show the structural and thermal characteristics of the PVA membranes. Figure 3a displays the chemical structure of PVA as well as the three-dimensional (3D) drawing of the chain molecules. PVA is known to have a monoclinic structure (Gupta et al., 2009). Hence, as shown in Figure 3b, the typical (101) peak is observed at $2\theta \approx 19.7°$ whereas the small peak at $2\theta \sim 38°$ is ascribed to the presence of impurity during the chemical processes. Importantly, the crystallite size (t) could be estimated from Scherrer's relation, $t = 0.9 \cdot \lambda / (\beta \cdot \cos\theta)$, where λ (= 0.154 nm) is the x-ray wavelength, β is the full width at

half maximum (FWHM), and θ is the x-ray diffraction angle. Accordingly, when β is 0.046251 radians, θ is 19.7°, the crystallite size in the PVA membrane is about 3 nm (the PVA membrane looks transparent externally because of this small crystallite size, less than visible wavelength of ~400-800 nm). Furthermore, Figures 3c and d display the thermogravimetric analysis (TGA) and differential thermal analysis (DTA) data for the pure PVA and the PVA/Na_2SO_4 membranes, respectively.

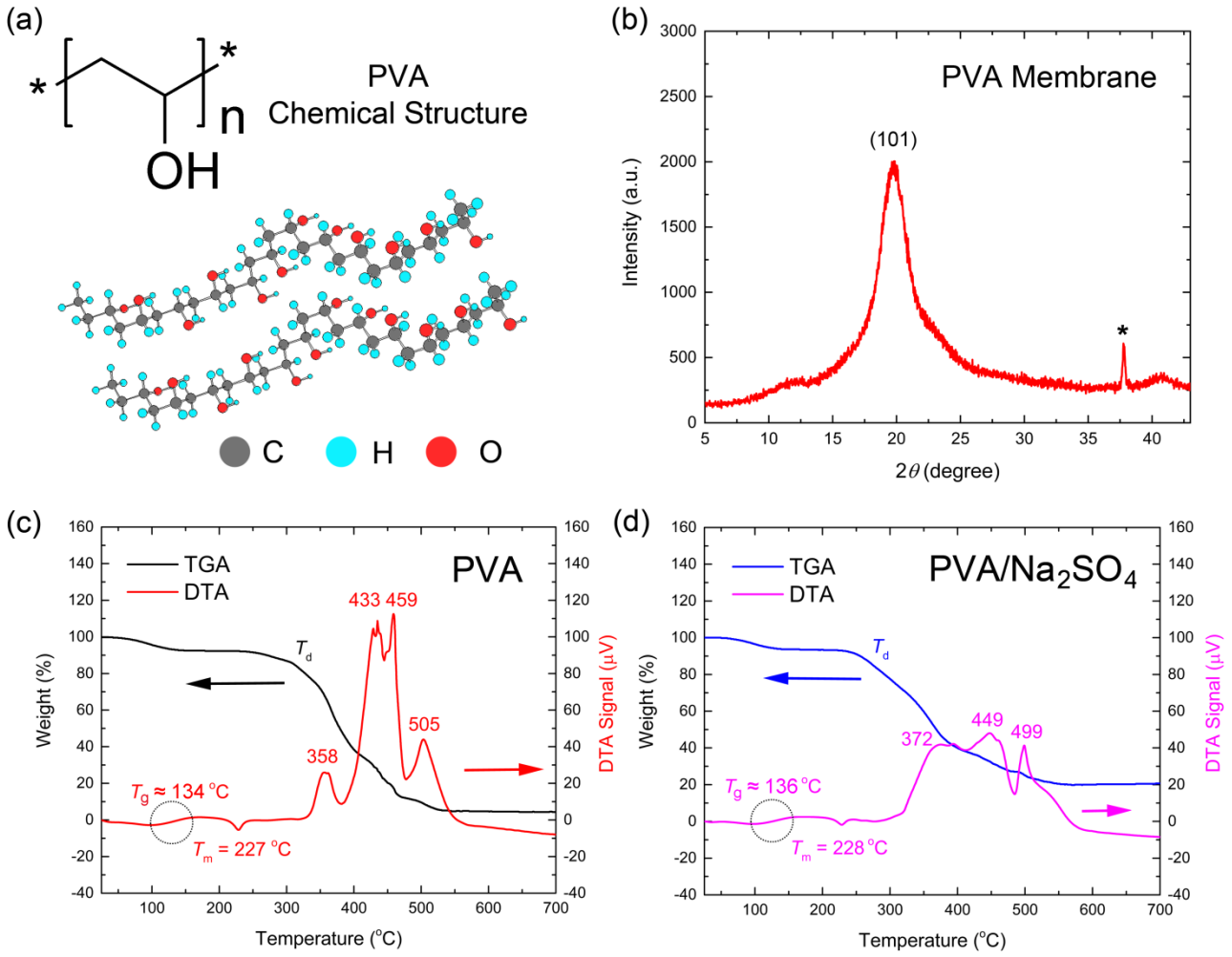

Figure 3. (a) Chemical structure of PVA macromolecule, (b) XRD patterns of PVA membrane; the star mark peak is from impurity, (c) TGA and DTA data of PVA membrane, and (d) TGA and DTA data of PVA/Na_2SO_4 (= 40:1 wt. ratio sample) membrane.

First, in the TGA data, the initial weight loss from RT to ~100 °C is related to the evaporation of water (less than 10 wt.%) from the hygroscopic PVA and PVA/Na_2SO_4 membranes, whereas the weight loss at T_d (decomposition temperature) ~ 300-500 °C originates from the thermal decomposition of these organic molecules. However, as shown in DTA data, if we see the detail, the PVA/Na_2SO_4 sample (Figure 3c and d) exhibits the different decomposition mechanism compared to the pure PVA, demonstrating the effect of sodium salt on the thermal decomposition properties of materials. Here, the sodium ions are able to have coordination bonding with the oxygen atom of PVA because the loan pair electrons in oxygen (Lewis's base) acts as electron donor whereas the sodium cation (Lewis's acid) acts as electron acceptor, i.e., so called 'the acid-base reaction'. On the other hand, SO_4^{2-} anions might be distributed in the PVA matrix because Na^+ is complexed with –O-H moiety. Here, it is well known that the ionic conductivity is available because of the segmental movement of polymer as well as the dissolved cations coordinated with the Lewis

base moiety (Kim, 2022; Mengistie et al., 2021). Interestingly, DTA data displays the clear melting point (T_m) of PVA at ~227-228 °C. Note that the minus signal of DTA indicates the endothermic reaction (e.g., phase transition due to the melting phenomena). In the case of the glass transition temperature (T_g), PVA shows T_g ~134 °C at the center of 113 °C and 155 °C (see the black dotted circle for clarity) whereas PVA/Na_2SO_4 displays T_g ~ 136 °C at the center of 114 °C and 158 °C. However, these values might include the thermal history of samples. Hence, if one would like to obtain the precise T_g data, it could be obtained by heating and cooling cycles through a sensitive differential scanning calorimetry (DSC) equipped with liquid nitrogen, which is not available in our laboratory. Furthermore, regarding the decomposition temperature (T_d) of samples, PVA shows T_d ~ 321 °C whereas PVA/Na_2SO_4 displays T_d ~ 289 °C when decided at the 20% loss of samples, indicating the pure PVA is thermally more stable than the PVA/Na_2SO_4 mixture.

Figure 4 shows the optical microscopy (OM) images of the phase-inversion membranes, (a) the pure PVA and (b) PVA/Na_2SO_4 thin films, respectively. As shown in Figure 4, we can find the microscale pores which should be constructed when water molecules were escaped from the PVA by help of the ethanol molecules. Furthermore, the removal of H_2O from the PVA thin film should be more active at the surface than the buried bottom part, providing the inescapable asymmetric structure with micro/nano pores, i.e., utilizable for many technical applications including filtration and separation (Loeb & Sourirajan, 1963; Wienk et al., 1996). However, the higher resolution scanning electron microscopy (SEM) and transmission electron microscopy (TEM) are not available in our Lab, limiting the nano-/micro-scale clear image capture in this study, which will be included in the future works.

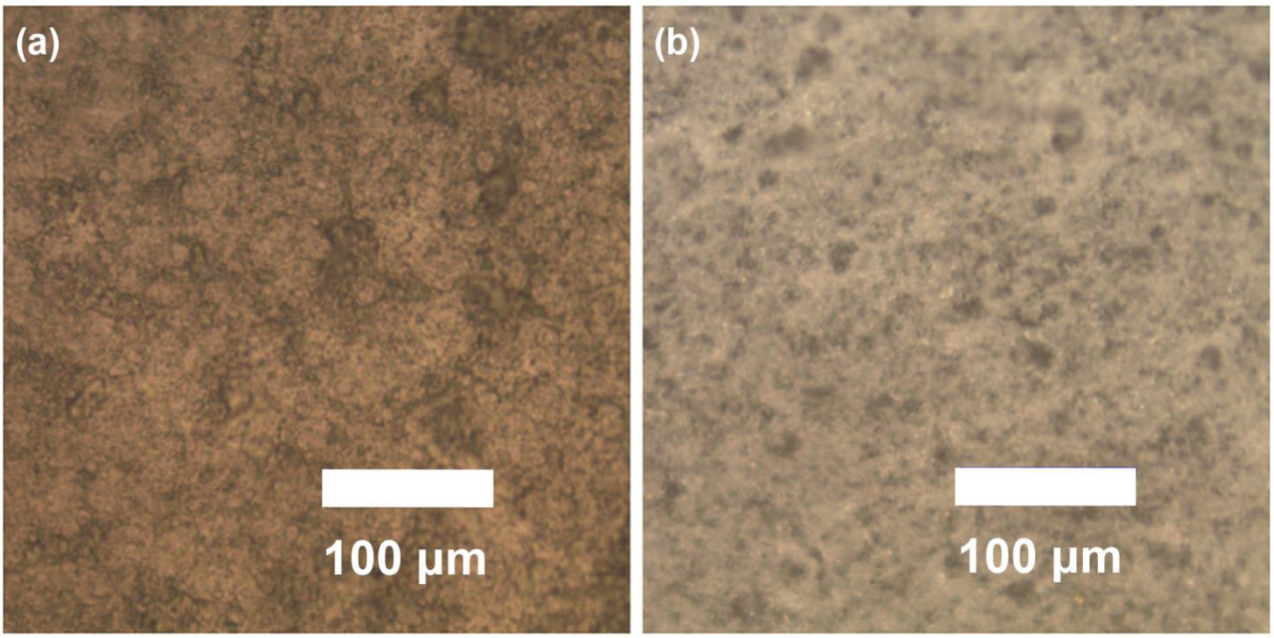

Figure 4. Optical microscopy images of the phase-inversion membranes: (a) pure PVA and (b) PVA/Na_2SO_4.

Figure 5 shows the electrochemical analysis set up (Figure 5a-d) and the resulting experimental data (Figure 5e-g). Figure 5e shows the Nyquist plot, providing the ionic conductivity data for the polymer electrolyte membrane. As shown in Figure 5e, we cannot observe a clear half circle with the spike, indicating the ionic conductivity of the PVA-based polymer electrolyte might be low. Accordingly, by extrapolating the spike to the x-axis as indicated by the blue dashed line, we could estimate the ionic conductivity (σ) based on

the equation, $\sigma = L/(R_b \cdot A)$ (Kim, 2022; Mengistie et al., 2021), where L (≈ 125 μm = 0.0125 cm) is the thickness, R_b is the bulk resistance, and A (= 4 cm^2) is the area of the membrane, respectively. Here note that the thickness of films could be measured using the optical microscopy with the configuration of glass/PVA (vertical direction)/glass. Hence, when $R_b \approx 15,000\,\Omega$ (0.5 M) and $R_b \approx 16,000\,\Omega$ (1.0 M), the ionic conductivity is 1.9×10^{-7} S/cm and 2.0×10^{-7} S/cm, respectively, which falling into the semiconductor's conductivity. Importantly, for being applied to the commercial batteries, the ionic conductivity of electrolyte should be comparable to that of liquid electrolyte (~10^{-2} S/cm, at least more than 10^{-4} S/cm). However, beyond the energy storage and conversion devices, there might be other applications such as electrochemical sensors because water-soluble PVA allows a green process, environmentally-friendly. Finally, it is noteworthy that the observed low ionic conductivity (= charge × mobility) might be mainly related to the solid-state film (a limited chain motion and concomitantly slow ionic transport) without any plasticizer like in gel polymer electrolyte (Gu & Wei, 2016; Wang et al., 2024; Sánchez-Valdez et al., 2023; Xiao et al., 2021; Taktar et al, 2020; Xie et al., 2020; Cheng et al., 2019; Li et al., 2018; Pendashteh et al., 2017; Batisse & Raymundo-Piñero, 2017). Other minor factors might be not sufficient free ions through ionic association in the solid-state films because there is no additive with high dielectric constant (Kim, 2022). On the other hand, Figure 2f shows the charge density vs. voltage plot. Here, through the integration of the area (i.e., closed circle), we may estimate the energy $\left[= \int Q(V) \cdot V\, dV\right]$. Resultantly, we obtained 9.2 μJ/cm^2 and 8.1 μJ/cm^2 for the PVA (Na_2SO_4 0.5M) and PVA (Na_2SO_4 1.0 M), respectively. Furthermore, Figure 2g shows the areal capacitance vs. voltage plot, displaying the areal capacitance in the range of ± 10 μF/cm^2 (based on the active area of 2×2 cm^2, i.e., the overlapped region of ITO glasses; see the inset of Figure 5e) which is a reasonable value because it depends only on the electric double layer capacitance (EDLC) without any pseudocapacitance from the redox reaction. Here, EDLC should be dependent on the two-dimensional (2D) interface between ITO and PVA in the solid state.

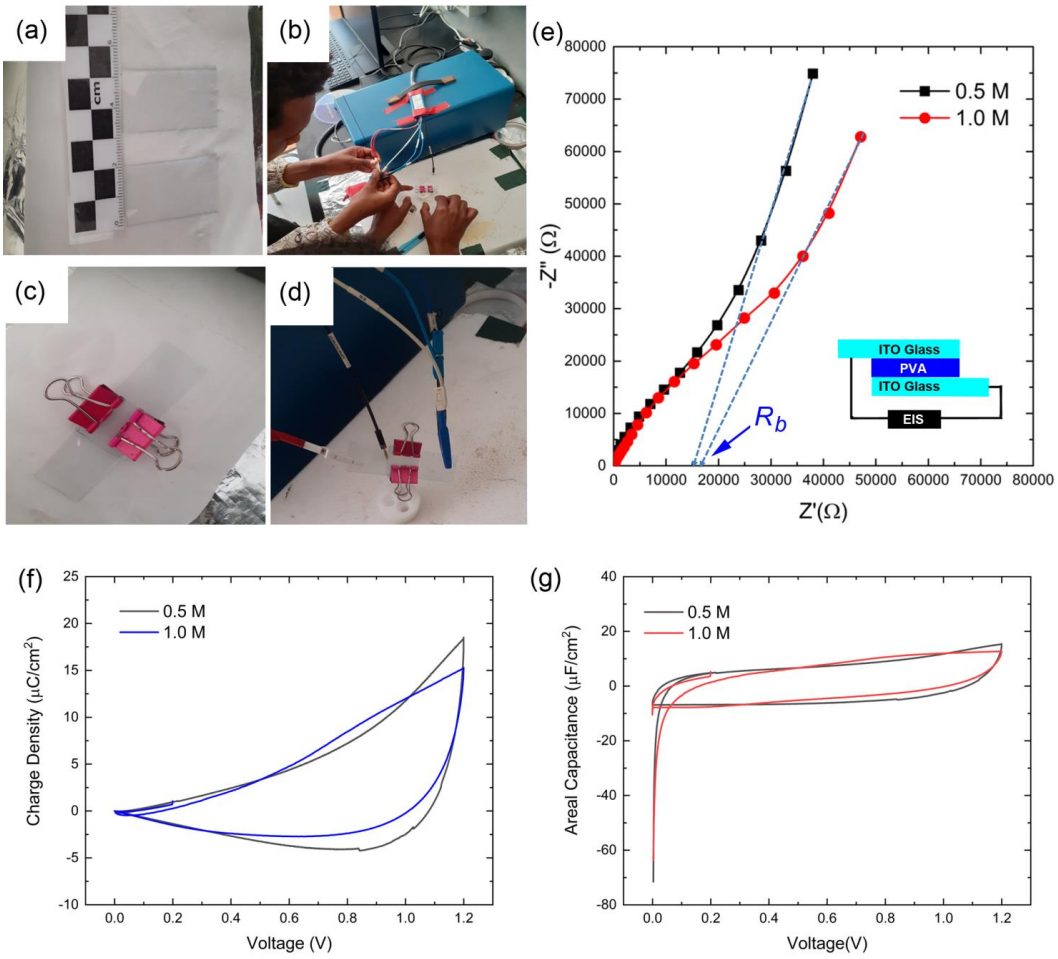

Figure 5. (a) ITO Glass, (b) EIS measurement, (c) Device structure, (d) Current-voltage curve measurement system, (e) Nyquist plot with the inset showing the schematic device structure, (f) Charge density vs. Voltage, and (g) Areal capacitance vs. Voltage at the scan rate of 50 mV/sec. Here, (c) and (d) were calculated from the current-voltage plot when the active area is 4 cm^2 in the device configuration of ITO/PVA (Na_2SO_4, 0.5M or 1 M)/ITO. The device's active size was 2 cm × 2 cm as shown in Figure 5c.

3. Conclusions

Poly(vinyl alcohol)-based phase inversion membranes was prepared to be used as sodium-ion conducting solid polymer electrolyte (SPE). The asymmetric membranes displayed when ethanol and water were exchanged in the phase inversion process. The PVA membrane has a monoclinic structure with the characteristic (101) peak at 2θ= 19.7 °, and has a melting point at ~207–208°C with the major thermal decomposition in the range of ~300–500 °C as usual for organic molecules. Finally, the PVA/Na_2SO_4–based SPE displayed its ionic conductivity of ~ 10^{-7} S/cm, which is not surprising because it is in the solid state, suggesting a potential future work for enhancing its ionic conductivity through additive engineering using plasticizers and fillers. Interestingly, when we fabricated the electrochemical devices with the configuration of ITO/PVA(Na_2SO_4)/ITO, it showed the EDLC capacitor behavior with the potential energy storage of 9.2 μF/cm^2 (0.5M) and 8.1 μF/cm^2 (1.0 M) in the voltage scan range of 0.0V to 1.2 V.

Author Contributions: writing—original draft preparation, L.M., L.S., L.D., and M.M..; data curation, L.M., L.S., L.D., and M.M..; writing—review and editing, J.Y.K.; supervision, J.Y.K. All authors have read and agreed to the published version of the manuscript.

Funding: This research received no external funding

Acknowledgments: The project (EDCF L/A No. ETH-6) entitled "Establishment of Centers of Excellence for Adama Science and Technology University" is appreciated, in which EDCF stands for Economic Development Cooperation Fund (a loan aid) provided from the Korean government to Ethiopia.

Conflicts of Interest: The authors declare no conflicts of interest.

References

Ahmad, A. L.; Yusuf, N. M.; Ooi, B. S. (2012). Preparation and Modification of Poly (Vinyl) Alcohol Membrane: Effect of Crosslinking Time towards Its Morphology. Desalination, 287, 35–40. https://doi.org/10.1016/j.desal.2011.12.003.

Bae, B.; Kim, D. (2021). Polymer Electrolyte Membranes. Membranes, 11, 244. https://doi.org/10.3390/membranes11040244.

Batisse, N.; Raymundo-Piñero, E. (2017). A self-standing hydrogel neutral electrolyte for high voltage and safe flexible supercapacitors. J. Power Sources, 348, 168-174. https://doi.org/10.1016/j.jpowsour.2017.03.005.

Cheng, B.; Cheng, R.; Tan, F.; Liu, X.; Huo, J.; Yue, G. (2019). Highly Efficient Quasi-Solid-State Asymmetric Supercapacitors Based on MoS2/MWCNT and PANI/MWCNT Composite Electrodes. Nanoscale Res. Lett., 14, 66. https://doi.org/10.1186/s11671-019-2902-5

Drioli, E.; Fontananova, E. (2012) Membrane Materials for Addressing Energy and Environmental Challenges. Annu. Rev. Chem. Biomol. Eng., 3, 395–420. https://doi.org/10.1146/annurevchembioeng-062011-081027.

Eljaddi, T.; Giordano, L.; Roizard, D. (2021). Towards the Synthesis of Greener Membranes: Interest of PVA as Porous Support for Membrane Application in Gas and Liquid Separations. Sep. Purif. Technol., 263, 118357. https://doi.org/10.1016/j.seppur.2021.118357.

Gu, T.; Wei, B. (2016). High-performance all-solid-state asymmetric stretchable supercapacitors based on wrinkled MnO2/CNT and Fe2O3/CNT macrofilms. J. Mater. Chem. A, 4, 12289-12295. https://doi.org/10.1039/C6TA04712B.

Guillen, G. R.; Pan, Y.; Li, M.; Hoek, E. M. V. (2011). Preparation and Characterization of Membranes Formed by Nonsolvent Induced Phase Separation: A Review. Ind. Eng. Chem. Res., 50, 3798–3817. https://doi.org/10.1021/ie10192.

Gupta, S.; Pramanik, A.K.; Kailath, A.; Mishra, T.; Guha, A.; Nayar, S.; Sinha, A. (2009). Composition dependent structural modulations in transparent poly(vinyl alcohol) hydrogels. Colloids Surf. B Biointerfaces, 74, 186–190. https://doi.org/10.1016/j.colsurfb.2009.07.015.

Hong, S.U.; Kim, J.Y.; Kang, Y.S. (2001). Effect of feed pressure on facilitated olefin transport through solid polymer electrolyte membranes. Polym. Adv. Technol., 12, 177-182. https://doi.org/10.1002/pat.128.

Kahrs, C.; Schwellenbach, J. (2020). Membrane Formation via Non-Solvent Induced Phase Separation Using Sustainable Solvents: A Comparative Study. Polymer, 186, 122071. https://doi.org/10.1016/j.polymer.2019.122071.

Kamcev, J.; Freeman, B. D. (2016). Charged Polymer Membranes for Environmental/Energy Applications. Annu. Rev. Chem. Biomol. Eng., 7, 111–133. https://doi.org/10.1146/annurev-chembioeng-080615-033533.

Katkar, P.K.; Marje, S.J.; Pujari, S.S.; Khalate, S.A.; Deshmukh, P.R.; Patil, U.M. (2020). Single-pot hydrothermal synthesis of manganese phosphate microrods as a cathode material for highly stable flexible solid-state symmetric supercapacitors. Synth. Met., 267, 116446. https://doi.org/10.1016/j.synthmet.2020.116446.

Kim, J.Y. (2022). Phase behavior of binary and ternary fluoropolymer (PVDF-HFP) solutions for single-ion conductors. RSC Adv., 12, 21160-21171. https://doi.org/10.1039/D2RA04158H.

Kim, J.Y.; Bae, Y.C. (1999a). Configurational entropy effect for conductivities of solid polymer electrolytes. J. Appl. Polym. Sci., 73, 1891-1897. https://doi.org/10.1002/(SICI)1097-4628(19990906)73:10<1891::AID-APP8>3.0.CO;2-M.

Kim, J.Y.; Bae, Y.C. (1999b). Configurational entropy effect for the conductivity of semicrystalline polymer/salt systems. Fluid Phase Equilib., 163, 291-302. https://doi.org/10.1016/S0378-3812(99)00230-7.

Kim, J.Y.; Chung, I.J. (2002). An All-Solid-State Electrochemical Supercapacitor Based on Poly3-(4-fluorophenylthiophene) Composite Electrodes. J. Electrochem. Soc., 149, A1376. https://doi.org/10.1149/1.1506301.

Kim, J.Y.; Chung, I.J.; Kim, J.K.; Yu, J.-W. (2006). Solid-state photovoltaic devices based on perylene acid-sensitized nanostructural SnO2 with P(VdF-co-HFP) gel electrolyte. Curr. Appl. Phys., 6, 969-973. https://doi.org/10.1016/j.cap.2005.05.003.

Li, X.; Shao, J.; Kim, S.-K.; Yao, C.; Wang, J.; Miao, Y.-R.; Zheng, Q.; Sun, P.; Zhang, R.; Braun, P.V. (2018). High energy flexible supercapacitors formed via bottom-up infilling of gel electrolytes into thick porous electrodes. Nat. Commun., 9, 2578. https://doi.org/10.1038/s41467-018-04937-8.

Loeb, S.; Sourirajan, S. (1963). Sea Water Demineralization by Means of an Osmotic Membrane. Adv. Chem. Ser., 38, 117–132. https://doi.org/10.1021/ba-1963-0038.ch009.

Long, L.; Wang, S.; Xiao, M.; Meng, Y. (2016). Polymer electrolytes for lithium polymer batteries. J. Mater. Chem. A, 4, 10038-10069. https://doi.org/10.1039/C6TA02621D

Mengistie, T.S.; Ko, J.M.; Kim, J.Y. (2021). Enhanced single-ion conduction and free-standing properties of solid polymer electrolyte by incorporating a polyelectrolyte. Mater. Res. Express, 8, 035308. https://doi.org/10.1088/2053-1591/abee01

Pendashteh, A.; Senokos, E. ; Palma, J.; Anderson, M. ; Vilatela, J.J.; Marcilla, R. (2017). Manganese dioxide decoration of macroscopic carbon nanotube fibers: From high-performance liquid-based to all-solid-state supercapacitors. J. Power Sources, 372, 64-73. https://doi.org/10.1016/j.jpowsour.2017.10.068.

Sánchez-Valdez, A.G.; de la Parra-Arciniega, S.M.; Sánchez-Cervantes, E.M.; Torres-González, L.C. (2023). Neutral pH Na2SO4/glycerol/PVA polymer hydrogel electrolyte prepared at room temperature for activated carbon supercapacitors. J. Solid State Electrochem., 27, 2917–2925. https://doi.org/10.1007/s10008-023-05631-6.

Sapalidis, A. A. (2020). Porous Polyvinyl Alcohol Membranes: Preparation Methods and Applications. Symmetry, 12, 960. https://doi.org/10.3390/sym12060960.

Tavajohi, N.; Khayet, M. (2024) Polymeric Membrane Formation by Phase Inversion; Elsevier: Amsterdam, Netherlands.

Wang, D.-M.; Lai, J.-Y. (2013). Recent Advances in Preparation and Morphology Control of Polymeric Membranes Formed by Nonsolvent Induced Phase Separation. Curr. Opin. Chem. Eng., 2, 229–237. https://doi.org/10.1016/j.coche.2013.04.003.

Wang, Y.; Chen, K. S.; Mishler, J.; Cho, S. C.; Adroher, X. C. (2011) A Review of Polymer Electrolyte Membrane Fuel Cells: Technology, Applications, and Needs on Fundamental Research. Appl. Energy, 88, 981–1007. https://doi.org/10.1016/j.apenergy.2010.09.030.

Wang, Z.; Yang, J.; Yan, J.; Guo, Q.; Huang, L.; Cui, J.; Liu, J.; Zhang, Q.; Hu, X.; Wu, Y. (2024). A 2.3 V quasi-solid-state flexible supercapacitor of AC|PVA-Na2SO4// PVA-KOH| Zn@CFP with high specific energy. J. Energy Storage, 82, 110601. https://doi.org/10.1016/j.est.2024.110601.

Wienk, I.M.; Boom, R.M.; Beerlage, M.A.M.; Bulte, A.M.W.; Smolders, C.A.; Strathmann, H. (1996). Recent advances in the formation of phase inversion membranes made from amorphous or semi-crystalline polymers. J. Membr. Sci., 113, 361–371. https://doi.org/10.1016/0376-7388(95)00256-1

Xiao, K.; Yang, T.; Liang, J.; Rawal, A.; Liu, H.; Fang, R.; Amal, R.; Xu, H.; Wang, D.-W. (2021). Nanofluidic voidless electrode for electrochemical capacitance enhancement in gel electrolyte. Nat. Commun., 12, 5515. https://doi.org/10.1038/s41467-021-25817-8.

Xie, Y.; Zhang, H.; Huang, H.; Wang, Z.; Xu, Z.; Zhao, H.; Wang, Y.; Chen, N.; Yang, W. (2020). High-voltage asymmetric MXene-based on-chip micro-supercapacitors. Nano Energy, 74, 104928. https://doi.org/10.1016/j.nanoen.2020.104928.